ACS SyntheticBiology

Letter

pubs.acs.org/synthbio

In Vivo Gene Expression Dynamics of Tumor-Targeted Bacteria

Tal Danino,[†] Justin Lo,[†] Arthur Prindle,[‡] Jeff Hasty,[‡,§,∥] and Sangeeta N. Bhatia*[,†,⊥,¶,#,□]

[†]Health Sciences and Technology, Massachusetts Institute of Technology, Cambridge, Massachusetts 02139, United States

[‡]Department of Bioengineering, [§]Biocircuits Institute, and [∥]Molecular Biology Section, Division of Biological Science, University of California, San Diego, La Jolla, California 92093, United States

[⊥]Broad Institute of Harvard and MIT, Cambridge, Massachusetts 02142, United States

[¶]Department of Medicine, Brigham and Women's Hospital, Boston, Massachusetts 02115, United States

[#]Electrical Engineering and Computer Science and David H. Koch Institute for Integrative Cancer Research, Massachusetts Institute of Technology, Cambridge, Massachusetts 02139, United States

[□]Howard Hughes Medical Institute, Chevy Chase, Maryland 20815, United States

Supporting Information

ABSTRACT: The engineering of bacteria to controllably deliver therapeutics is an attractive application for synthetic biology. While most synthetic gene networks have been explored within microbes, there is a need for further characterization of *in vivo* circuit behavior in the context of applications where the host microbes are actively being investigated for efficacy and safety, such as tumor drug delivery. One major hurdle is that culture-based selective pressures are absent *in vivo*, leading to strain-dependent instability of plasmid-based networks over time. Here, we experimentally characterize the dynamics of *in vivo* plasmid instability using attenuated strains of *S. typhimurium* and real-time monitoring of luminescent reporters. Computational modeling described the effects of growth rate and dosage on live-imaging signals generated by internal bacterial populations. This understanding will allow us to harness the transient nature of plasmid-based networks to create tunable temporal release profiles that reduce dosage requirements and increase the safety of bacterial therapies.

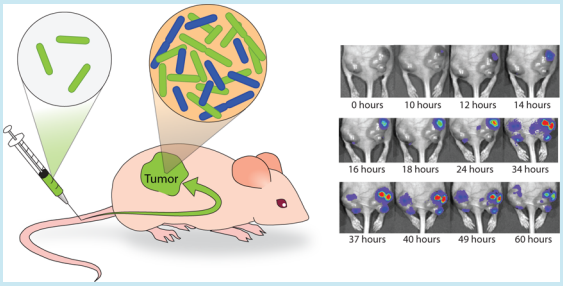

KEYWORDS: *synthetic biology, S. typhimurium, bacterial cancer therapy, plasmid-loss dynamics*

Over the past century, the observation that bacteria accumulate preferentially in tumors has prompted the investigation of the use of a number of strains for cancer therapy, including *C. novyi*, *E. coli*, *V. cholorae*, *B. longum*, and *S. typhimurium*.[3,13,2,27,17,24] Attenuated strains of *S. typhimurium* have generated particular interest as they can innately home to and colonize tumors of a variety of sizes and have exhibited safety and tolerance in human clinical trials.[25,5,22,8] *S. typhimurium* were initially shown to mediate antitumor effects through recruitment of the host immune system and by competition with cancer cells for nutrients. Subsequently, engineered production of therapeutic cargo was added through simple genetic modifications. While these studies represent important advances in the use of bacteria for tumor therapies, the majority of existing efforts have relied on constitutive, "always on" cargo production[9,26,16,6] that typically results in the delivery of high dosages, off-target effects, and development of host resistance.

As a next step, synthetic biology seeks to add controlled and dynamic production of cargo by utilizing computationally designed "circuits" that have sophisticated sensing and delivery capabilities.[7,4,19,1] These circuits can be designed to act as delivery systems that sense tumor-specific stimuli and self-regulate cargo production as necessary. Since plasmids are the common framework for synthetic circuits, we begin by characterizing the dynamics of plasmid-based gene expression in an *in vivo* mouse model by utilizing real-time luminescence imaging, quantitative biodistribution measurement, and computational modeling. Together, these approaches provide a framework for exploiting the inherent instability of plasmid-based networks, which will facilitate the generation of specific temporal release profiles directly within the tumor environment.

We began by transforming two different attenuated strains of *S. typhimurium* with a constitutively expressed luciferase plasmid (luxCDABE genes on a pBR322/colE1 high-copy without partitioning machinery) to allow for real-time monitoring of luminescence with an *in vivo* imaging system (IVIS).[13] Strain A (*ELH430*:SL1344 phoPQ-) is attenuated for the PhoPQ regulon, which is known to activate a number of genes related to virulence, while Strain B (*ELH1301*:SL1344 phoPQ- aroA-) contains an additional aromatic amino acid synthesis mutation that effectively allows it to grow only in

Special Issue: Engineered Microbes for Therapeutic Applications

Received: July 12, 2012
Published: September 21, 2012

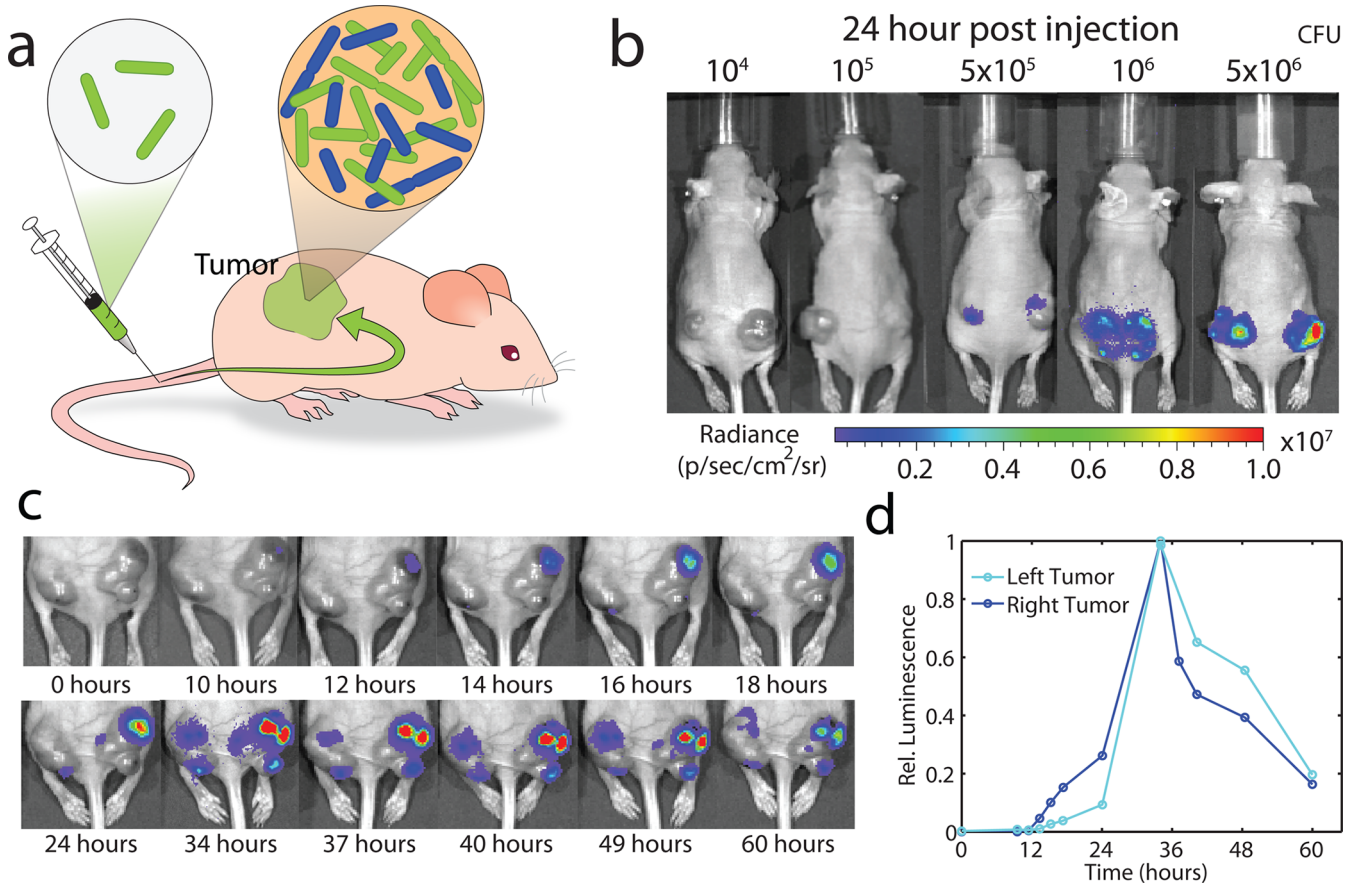

Figure 1. Tumor homing bacteria and dosage variation. (a) *S. typhimurium* are injected via tail vein into nude mice and localize to subcutaneous tumors where they replicate. (b) Dosages between 10^4 and 5×10^6 bacteria (Strain A) were injected into mice, and IVIS images were taken after 24 h. Higher initial dosages show an increasing signal and a minimum value of 5×10^5 bacteria required to visualize tumor colonization at 24 h. (c) Sequence of IVIS images for strain Strain A at 10^6 dosage over the course of 60 h. (d) Total flux of left (light blue) and right (dark blue) tumors as a function of time normalized to the maximum value across the trajectory. The IVIS signal rises due to rapid bacterial growth and then decays due to plasmid loss and luciferase instability.

nutrient-rich environments. Importantly, while these strains are derived from the same parent (SL1344), their growth rates and therefore plasmid-loss dynamics differ significantly. To investigate the *in vivo* gene expression dynamics of these strains, we generated model xenograft tumors in mice by subcutaneous injection of a human ovarian cancer cell line (OVCAR-8). After measurable tumors were established, bacterial strains were injected intravenously via tail vein (Figure 1a) with dosages varying from 10^4 to 5×10^6 bacteria. Once injected, bacteria specifically colonized tumors at a rate proportional to the dosage administered, as measured by IVIS signal at 24 h post-injection (Figure 1b).

We then monitored the tumor site for Strain A-derived signal over the course of 60 h using time-lapse IVIS imaging (Figure 1c,d). These trajectories followed the specific pattern of an initial steep increase followed by a gradual decrease back to baseline (Figure 1d). We hypothesized that the shape of this waveform was the result of the initial exponential growth of plasmid-containing bacteria followed by increasing rates of plasmid loss in the absence of antibiotic selection. Eventually, the rate of luciferase production by the remaining plasmid-containing bacteria is overtaken by luciferase decay, and the total signal begins to decline.

To test this hypothesis, we counted the number of plasmid-containing and non-plasmid-containing bacteria in tumors over time by observing bacterial growth on selective media (Strain A, 10^6 bacteria injected). Each measurement was compared to counts taken in the spleen, a control tissue where there a stable subpopulation is present, as the bacteria initially accumulate but do not grow or die in this site. At each time point, organs were excised from the mouse and then homogenized and plated with or without antibiotic selection (Figure 2a, $n = 3–5$ tumors). Colony counting on these plates yielded an accurate measure of the plasmid state of the bacterial population over time (Figure 2b). After 2 h, roughly 3×10^3 plasmid-containing bacteria reside in the tumor, or about 0.3% of the injected dose. After 12 h, plasmid-containing bacteria grow to a level of 10^6, and the number of non-plasmid-containing bacteria reaches a similar level. This accumulation corresponds to a doubling time of approximately 75 min. Growth rate declined further over time, presumably due to nutrient limitation, ultimately resulting in a 300 min doubling time for non-plasmid-containing bacteria (Figure 2b).

While the total population of bacteria grew throughout the course of the experiment (60 h), the number of plasmid-containing bacteria reaches a maximum at 24 h (Figure 2b). By taking the ratio of these populations, we can calculate the percentage of plasmid-containing bacteria over time (Figure 2c). After 12 h, roughly 50% of the population retains the plasmid, a fraction that drops to 10% after 24 h (Figure 2c). The slope of this line remains constant throughout the 60-h

dx.doi.org/10.1021/sb3000639 | *ACS Synth. Biol.* 2012, 1, 465–470

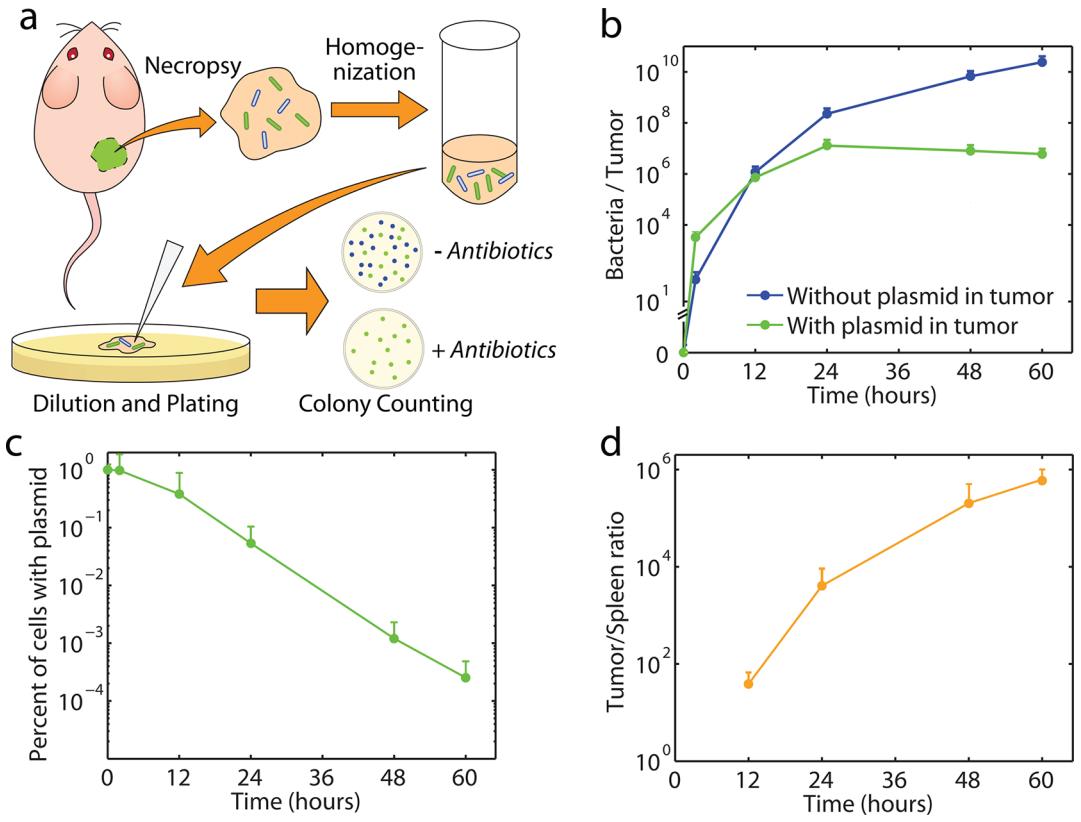

Figure 2. Population dynamics of bacteria inside tumor environments. (a) Schematic showing tumor extraction, homogenization, and plating to count internal populations of bacteria. Plating on antibiotics reveals the number of plasmid-containing bacteria, while plating without antibiotics gives the total number of bacteria. (b) Measured number of plasmid-containing and non-plasmid-containing bacteria per organ calculated for plasmid-containing bacteria (green) and non-plasmid-containing bacteria (blue). Bacteria with the plasmid reach a steady state around 24 h, while the non-plasmid bacteria continue to grow. (c) Percentage of cells containing the plasmid as a function of time showing a constant loss rate over the course of 72 h. (d) Ratio for total number of bacteria in the tumor versus the spleen. This number is typically reported as a measure of specificity of the tumor-targeting strain. Strain A at a dosage of 10^6 cells was used for all panels. Lines indicate a piecewise linear fit of the data.

experiment and represents the rate of plasmid loss in the tumor environment.

The tumor-spleen ratio is commonly reported as a characteristic measure of specificity and tumor-homing ability for a given strain. Bacteria accumulate in the spleen from the initial dosing yet do not subsequently grow and divide. Given that we observed essentially no increase in the bacterial count in the spleen throughout the duration of our experiments, the tumor-spleen ratio increased over time (Figure 2d). Since this ratio is typically reported as a fixed number in the literature, its time-dependence may help to explain the wide range of reported values.[14,23]

To explore how bacterial growth rate affects the dynamics of plasmid instability over time, we injected two groups of mice with Strain A and B (at a dosage of 10^6) and monitored their signal over the course of 60 h. The two strains displayed markedly different profiles, with Strain A peaking and decaying sharply and the slower growing Strain B peaking broadly over a longer period of time before decaying (Figure 3a,b). We plot the average trajectories for Strains A and B on an absolute luminescence scale in Figure 3c for comparison. To quantify these differences, we measured the width at half-maximum and total area under each curve for the average trajectories (Figure 3d). These measurements illustrate that Strain A produces more luminescence quickly while Strain B produces less luminescence over a longer period of time (Figure 3d). Additionally, to confirm that signal intensity is a representative measure of the population of plasmid-containing bacteria, we compared counts of antibiotic resistant bacteria with absolute IVIS values at the 72-h time point and found them to be highly correlated (R = 0.832, Supporting Information).

Developing a fully tunable dynamic expression platform will require a more complete understanding of the underlying processes. Plasmid-loss dynamics have been well described in a variety of *in vitro* and *in vivo* contexts;[20,12,15] however, modeling of population or gene-expression dynamics has not yet been studied for *in vivo* tumor environments. Specifically, we hope to learn how expression dynamics are dictated by the rates of growth and plasmid-loss for a given strain. To accomplish this, we developed an ordinary differential equation (ODE) model describing internal plasmid and non-plasmid-containing bacteria and their respective expression of luciferase signal (Figure 4a). Initially, N_0 bacteria are injected. These plasmid-containing bacteria replicate and lose their plasmids at rate τ, resulting in populations of plasmid (N^+) and non-plasmid (N^-) containing bacteria that continue to grow at rates $\mu+$ and $\mu-$, respectively (Figure 4a). Both populations grow exponentially for 24 h until available nutrients become limiting, a process modeled by including a finite quantity of tumor substrate that is consumed according to Michaelis–Menten kinetics [21]. The tumor environment is also spatially restrictive of bacterial growth, with bacteria in the center consuming nutrients more slowly than bacteria on the rapidly growing periphery. Thus, despite a nearly constant population of plasmid-containing bacteria, IVIS

dx.doi.org/10.1021/sb3000639 | *ACS Synth. Biol.* 2012, 1, 465–470

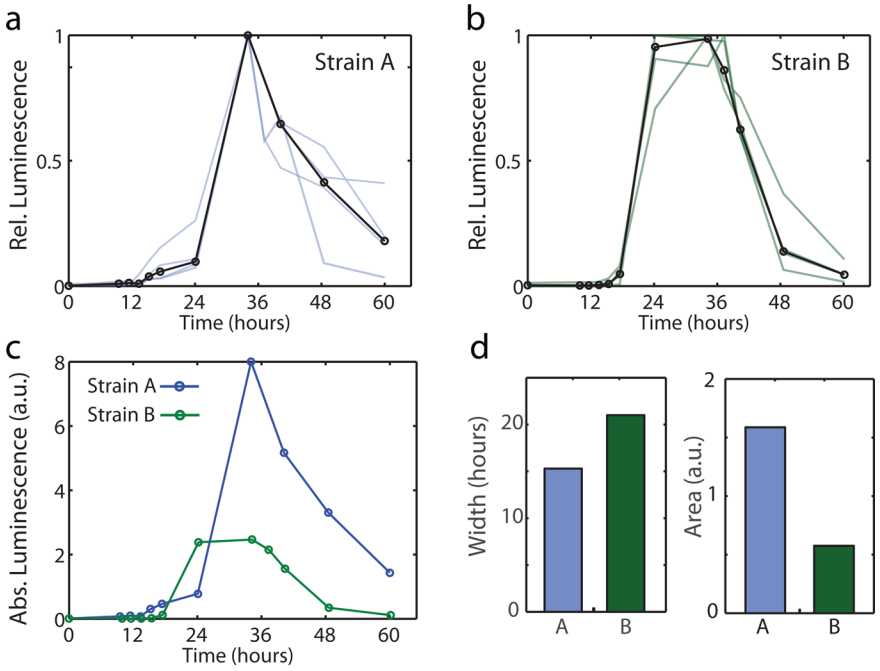

Figure 3. Characterization of Strain A and Strain B IVIS profiles. (a, b) Time-course trajectories for Strain A (a) and Strain B (b) over the course of 60 h normalized to their maximum value across the trajectory. Colored lines indicate individual trajectories, and the solid black line indicates the average trajectories. (c) Time-course trajectories for Strain A and Strain B on an absolute scale. Average trajectories from (a) and (b) were scaled by the average absolute value of the individual trajectories. (d) (left) Full-width at half-maximum and the area (right) under the curve for the average trajectory of both strains. These parameters characterize the dosage and duration of transient gene-expression.

signal fails to increase after 24 h since most of these bacteria reside in the non-growing center of the colony. We accounted for this behavior by limiting the amount of bacteria that can consume the tumor substrate, which effectively limits plasmid-containing bacterial growth and allows luciferase decay to dominate.

Our ODE model produced dynamics that were consistent with our experimental observations, where IVIS signal is taken to be proportional to the plasmid-containing population (Figure 4b). We define the full-width at half-maximum, ω, and area under the curve as important parameters that characterize the duration and magnitude of dosage, respectively (Figure 4c). To understand how to tune *in vivo* expression profiles according to these parameters, we varied growth rate and dosage level and modeled the effects on IVIS signal in each case (Figure 4d,e). Lower growth rates yield IVIS curves that are shifted toward later times with broader widths and lower areas (Figure 4d). In contrast, larger initial dosages result in a linear increase of IVIS signal that increases area but does not alter the width (Figure 4e). The latter linear increase in area as a function of dosage is reflective of doses much lower than the carrying capacity of the system. Finally, decreasing the plasmid-loss rate resulted in an increase in area under the curve as well as a slight shift in the width and time to peak of the gene expression profile (Supporting Information).

These effects correlate with experimental observations that can be explained based on differences in strain growth rate. Since plasmids are lost during cell division, the faster a cell replicates, the more frequently it loses plasmid. Thus, the faster growing Strain A accumulates luciferase quickly but loses a comparatively larger fraction of plasmids per day, resulting in higher IVIS values that peak at earlier time points than Strain B (Figure 3a,b). In contrast, Strain B grows more slowly, producing less luciferase but maintaining its plasmids much longer, yielding a broader expression profile compared to Strain A (Figure 3a,b).

In the context of drug delivery, a critical parameter is the rate at which a device releases drug into the surrounding environment. For instance, materials have been investigated that generate "burst", "delayed", or "sustained" release characteristics.[11] The transient plasmid-based system we have developed here can generate a similar variety of expression dynamics. For instance, Strain A produces an expression profile analogous to burst release due to its fast growth rate and high rate of plasmid loss. In contrast, Strain B yields a sustained release profile owing to its slow growth rate and moderate rate of plasmid loss. Bacteria are unique in the context of drug-delivery vehicles in that they produce their own cargo, in contrast to other devices that are preloaded and depleted. This difference allows them to deliver a time-varying concentration of cargo in a designed profile directly on site. In the future, this work will enable a variety of drug-release profiles from engineered bacteria for therapeutic applications.

Developing both experimental and computational techniques in concert will be critical to engineering *in vivo* genetic circuits.[7] Computational modeling can rapidly probe system parameters to explore potential outputs but must remain closely tied to experimental results to remain relevant. On the other hand, *in vivo* experiments present the most direct application of engineered circuits, but involve long time scales and the results are often difficult to interpret. Here, we have utilized plasmid instability to generate transient expression profiles in tumor environments. In our computational model, we can predict how dosage, strain growth rate, and plasmid loss rate combine to yield differing expression dynamics. Subsequently, these designs can be implemented experimentally by varying plasmid type, copy number, and maintenance system[18] or by modifying the strain growth rate. Building on this platform, future applications

dx.doi.org/10.1021/sb3000639 | *ACS Synth. Biol.* 2012, 1, 465–470

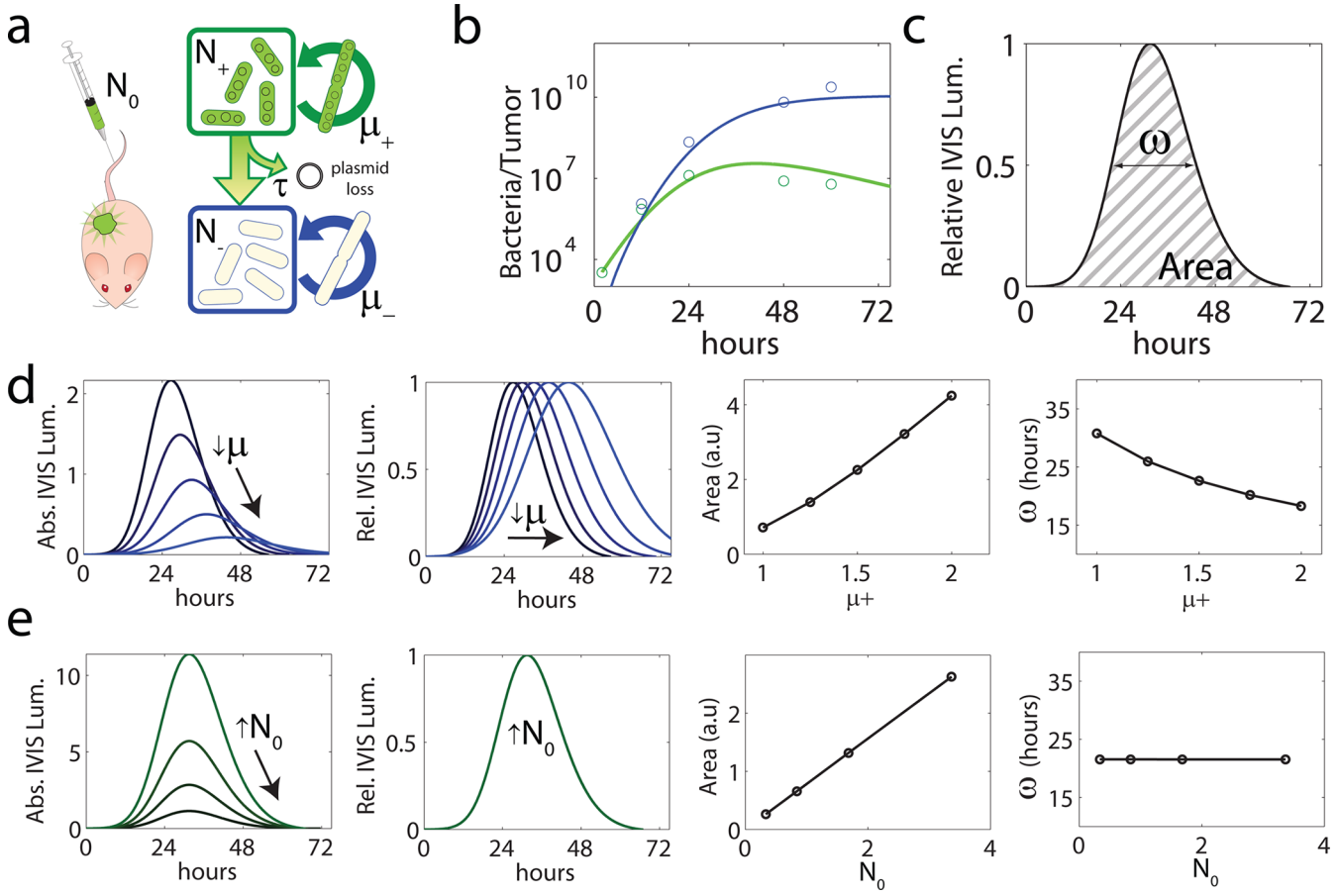

Figure 4. Modeling bacterial dynamics inside of tumor environments. (a) Schematic of mathematical model. Bacteria containing plasmids are injected at a dosage N_0. Plasmids are lost from cells at a rate τ, and growth of resulting plasmid-containing and non-containing cells continues at $\mu+$ and $\mu-$, respectively. (b) Modeling results (solid lines) for the number of plasmid-containing (blue) and non-plasmid-containing (green) bacterial population data from Figure 2b. Open circles indicate experimental points. (c) Typical time course of an IVIS trajectory indicating parameters ω and area for characterizing transient gene expression. The relative IVIS trajectory is typically measured experimentally due to mouse-to-mouse variability, while the absolute IVIS trajectories are used to calculate ω and area. (d) The effect of growth rate on transient gene expression. Decreasing growth rate shifts the absolute IVIS signals to a lower value and longer peak times, therefore increasing ω and decreasing the area under the curve. (e) The effect of initial dosage on transient gene expression. Increasing the dosage shifts the absolute IVIS signals to a higher level, increasing the area under the curve, but does not change the relative IVIS trajectory shape or ω value.

will include engineered gene circuits that further extend the range of expression dynamics, sensing tumor-specific stimuli and self-regulating cargo production.

METHODS

S. typhimurium strains Strain A (SL1344 PhoPQ-) and Strain B (SL1344 PhoPQ- aroA-) were provided by Elizabeth Hohmann (MGH).[10] The constitutive plasmid bearing luxCDABE genes was received as a gift from the Weiss lab.[13] On the day of injection, bacteria containing plasmids were diluted 1/1000 into fresh LB media (Difco, 0.22 μm filtered) with antibiotics (Ampicillin 100 μg/mL) and grown up to OD_{600} = 0.4−0.6. Cells were then prepared by washing 4 times with PBS (0.22 μm filtered) and measured for OD_{600}. Colony counts were performed on the preparation as a calibration and cells were prepared at various concentrations for 100 μL injections.

Subcutaneous human xenograft tumors were generated by injecting 5 × 10^6 OVCAR-8 cells (NCI DCTD Tumor Repository, Frederick, MD) bilaterally into the hind flanks of 4-week-old female Ncr/Nu mice. Cells were grown to 80−100% confluency in RPMI 1640 media supplemented with 10% fetal bovine serum and antibiotics (100 μg/mL penicillin and 100 μg/mL streptomycin) before injection. Cells were pelleted and resuspended in phenol red-free DMEM with 15% reduced growth factor Matrigel (BD Biosciences). Tumors were allowed to grow for 10−20 days until tumor masses of 200−500 mg were reached.

Colony counts were measured by dissecting tumors and organs from mice, homogenizing using a Tissue-Tearor (BioSpec), and plating serial dilutions on LB and LB Ampicillin plates. Prior to imaging, mice were anesthetized with 2−3% isoflurane. IVIS signals were measured using the IVIS Spectrum imaging system (Caliper Life Sciences) with 1−60 s exposure times, and Living Image software (Caliper Life Sciences) was used for analysis. Data where the tumor had ulcerated or had low signal (maximum of trajectory did not reach above 10^6 radiance, or approximately <5× initial background) were not included. Error bars drawn are standard error.

ASSOCIATED CONTENT

Supporting Information

This information is available free of charge via the Internet at http://pubs.acs.org

dx.doi.org/10.1021/sb3000639 | ACS Synth. Biol. 2012, 1, 465−470

AUTHOR INFORMATION

Corresponding Author

*E-mail: sbhatia@mit.edu.

Notes

The authors declare no competing financial interest.

ACKNOWLEDGMENTS

We thank members of the Bhatia lab for helpful discussions and H. Fleming for critical reading and editing of the manuscript. We thank E. L. Hohmann for providing strains ELH430 and ELH1301 as well as Sara Leschner and the Siegfried Weiss laboratory for providing the pluxCDABE plasmid. This work was supported by a Misrock Postdoctoral fellowship (T.D.), National Defense Science and Engineering Graduate Fellowship (A.P.), National Institute of Health Medical Scientist Training Program (J.L.), Ludwig Center for Molecular Oncology Graduate Fellowship (J.L.), and The Marie-D. & Pierre Casimir-Lambert Fund (J.L.). S.N.B is a HHMI Investigator.

REFERENCES

(1) Anderson, J. C., Clarke, E. J., Arkin, A. P., and Voigt, C. A. (2006) Environmentally controlled invasion of cancer cells by engineered bacteria. *J. Mol. Biol. 355* (4), 619−627.

(2) Cronin, M., Akin, A. R., Collins, S. A., Meganck, J., Kim, J. B., Baban, C. K., Joyce, S. A., van Dam, G. M., Zhang, N., van Sinderen, D., O'Sullivan, G. C., Kasahara, N., Gahan, C. G., Francis, K. P., and Tangney, M. (2012) High resolution in vivo bioluminescent imaging for the study of bacterial tumour targeting. *PloS One 7* (1), e30940.

(3) Dang, L. H., Bettegowda, C., Huso, D. L., Kinzler, K. W., and Vogelstein, B. (2001) Combination bacteriolytic therapy for the treatment of experimental tumors. *Proc. Natl. Acad. Sci. U.S.A. 98* (26), 15155.

(4) Danino, T., Mondragón-Palomino, O., Tsimring, L., and Hasty., J. (2010) A synchronized quorum of genetic clocks. *Nature 463* (7279), 326−330 PMID: 20090747..

(5) Forbes, N. S. (2010) Engineering the perfect (bacterial) cancer therapy. *Nat. Rev. Cancer 10* (11), 785−794.

(6) Guo, H., Zhang, J., and Inal, C. (2010) Targeting tumor gene by shrna-expressing salmonella-mediated rnai. *Gene Therapy 18* (1), 95−105.

(7) Hasty, J, McMillen, D, and Collins, J. J. (2002) Engineered gene circuits. *Nature 420* (6912), 224−230.

(8) Heimann, D. M., and Rosenberg, S. A. (2003) Continuous intravenous administration of live genetically modified salmonella typhimurium in patients with metastatic melanoma. *J. Immunother. 26* (2), 179.

(9) Hoffman, R. M. (2011) Tumor-seeking salmonella amino acid auxotrophs. *Curr. Opin. Biotechnol. 22* (6), 917−923.

(10) Hohmann, E. L., Oletta, C. A., and Miller, S. I. (1996) Evaluation of a phop/phoq-deleted, aroa-deleted live oral salmonella typhi vaccine strain in human volunteers. *Vaccine 14* (1), 19−24.

(11) Huang, X., and Brazel, C. S. (2001) On the importance and mechanisms of burst release in matrix-controlled drug delivery systems. *J. Controlled Release 73* (2), 121−136.

(12) Keesla, M., Peter, R., Donald, L., and Scott, W. (2009) Photonic plasmid stability of transformed salmonella typhimurium: A comparison of three unique plasmids. *BMC Microbiol.*, 9.

(13) Leschner, S., Westphal, K., Dietrich, N., Viegas, N., Jablonska, J., Lyszkiewicz, M., Lienenklaus, S., Falk, W., Gekara, N., Loessner, H., et al. (2009) Tumor invasion of salmonella enterica serovar typhimurium is accompanied by strong hemorrhage promoted by tnf-α. *PloS One 4* (8), e6692.

(14) Lm, Z., Luo, X., Feng, M., Li, Z., Ittensohn, M., Trailsmith, M., Bermudes, D., Lin, S. L., and King, I. C. (2001) Tumor amplified protein expression therapy: Salmonella as a tumor-selective protein delivery vector. *Oncol. Res. 12* (3), 127−135.

(15) Menanteau-Ledouble, S. (2010) *Pathogen entrance and development of disease during infection of the American channel catfish Ictalurus punctatus by the enterobacterium Edwardsiella ictaluri*, PhD thesis, Mississippi State University.

(16) Nguyen, V. H., Kim, H. S., Ha, J. M., Hong, Y., Choy, H. E., and Min, J. J. (2010) Genetically engineered salmonella typhimurium as an imageable therapeutic probe for cancer. *Cancer Res. 70* (1), 18.

(17) Pawelek, J. M., Low, K. B., and Bermudes, D. (1997) Tumor-targeted salmonella as a novel anticancer vector. *Cancer Res. 57* (20), 4537.

(18) Pecota, D. C., Kim, C. S., Wu, K., Gerdes, K., and Wood, T. K. (1997) Combining the hok/sok, parde, and pnd postsegregational killer loci to enhance plasmid stability. *Appl. Environ. Microbiol. 63* (5), 1917−1924.

(19) Prindle, A., Samayoa, P., Razinkov, I., Danino, T., Tsimring, L. S., and Hasty., J. (2011) A sensing array of radically coupled genetic 'biopixels'. *Nature 481*, 39−44.

(20) Stephanopoulos, G., and Lapudis, G. R. (1988) Chemostat dynamics of plasmid-bearing, plasmid-free mixed recombinant cultures. *Chem. Eng. Sci. 43* (1), 49−57.

(21) Stewart, F. M., and Levin., B. R. (1977) The population biology of bacterial plasmids: a priori conditions for the existence of conjugationally transmitted factors. *Genetics 87* (2), 209−228.

(22) Toso, J. F., Gill, V. J., Hwu, P., Marincola, F. M., Restifo, N. P., Schwartzentruber, D. J., Sherry, R. M., Topalian, S. L., Yang, J. C., Stock, F., et al. (2002) Phase i study of the intravenous administration of attenuated salmonella typhimurium to patients with metastatic melanoma. *J. Clin. Oncol. 20* (1), 142.

(23) Xu, D. Q., Zhang, L., Kopecko, D. J., Gao, L., Shao, Y., Guo, B., and Zhao, L. (2009) Bacterial delivery of sirnas: a new approach to solid tumor therapy. *Methods Mol. Biol. 487*, 161−187.

(24) Yong, A. Y., Shabahang, S., Timiryasova, T. M., Zhang, Q., Beltz, R., Gentschev, I., Goebel, W., and Szalay, A. A. (2004) Visualization of tumors and metastases in live animals with bacteria and vaccinia virus encoding light-emitting proteins. *Nat. Biotechnol. 22* (3), 313−320.

(25) Zhao, M., Yang, M., Li, X. M., Jiang, P., Baranov, E., Li, S., Xu, M., Penman, S., and Hoffman, R. M. (2005) Tumor-targeting bacterial therapy with amino acid auxotrophs of gfp-expressing salmonella typhimurium. *Proc. Natl. Acad. Sci. U.S.A. 102* (3), 755.

(26) Zhao, M., Yang, M., Ma, H., Li, X., Tan, X., Li, S., Yang, Z., and Hoffman, R. M. (2006) Targeted therapy with a salmonella typhimurium leucine-arginine auxotroph cures orthotopic human breast tumors in nude mice. *Cancer Res. 66* (15), 7647.

(27) Zhou, S., Zhang, M., and Wang, J. (2011) Tumor-targeted delivery of tat-apoptin fusion gene using escherichia coli nissle 1917 to colorectal cancer. *Med. Hypotheses 76* (4), 533−534.

Mathematical model

Our ordinary differential equation model is presented below in non-dimensional form. The model describes the dynamics of two populations of bacteria, those containing the luminescent plasmid (n^+) and those who have lost the plasmid (n^-). The two populations grow inside the tumor environment and consume a substrate (S) which is in limited supply.

$$\frac{dn^+}{dt} = (1-\tau)\mu^+ n^+ - \gamma_+ n_+ \quad (1)$$

$$\frac{dn^-}{dt} = \mu^- n^- + \tau\mu^+ n^+ - \gamma_- n_- \quad (2)$$

$$\frac{dS}{dt} = -[\frac{\mu^- n^-}{A^-} - \frac{\mu^+ n^+}{A^+}][\frac{1}{1+q\cdot(n_- + n_+)}] \quad (3)$$

$$\mu^+ = \frac{\mu^+_{max} S}{K+S} \qquad \mu^- = \frac{\mu^-_{max} S}{K+S} \quad (4)$$

The parameters above are τ, the rate at which cells lose plasmid, μ^+_{max} and μ^-_{max}, the maximal growth of plasmid and non-plasmid containing cells respectively. K, the Michaelis-saturation constant of growth rate, A^+ and A^-, the depletion rate constants of substrate S by μ^+ and μ^- cells. γ_+ and γ_-, the death rates of the bacteria, and q, the rate at which tumor substrate depletion is limited by the maximal amount of cells. This last term is to account for the fact that a limited number of bacteria (those on the outward growing rim) can contribute to the decay of the tumor substrate. The model is non-dimensionalized by hours, 1 bacteria, and a substrate concentration of μM.

The total IVIS signal is reflective of the number of luciferase enzymes and hence the number of actively expressing luciferase bacteria. As an approximation to this signal, we modeled the signal to be proportional to the number of plasmid containing cells (dominant contribution to the IVIS signal) minus the first-order decay of the luciferase enzyme. We assume that each bacterium containing a plasmid contributes equally to the IVIS signal although there is likely variability due to the distribution of plasmids per cell in a population as well as contributions from non-plasmid containing bacteria where luciferase is not yet significantly diluted. Another approximation in the IVIS signal arises in that plasmid-containing bacteria initially populate the tumor core and express luciferase, but as bacteria grow radially to a larger population, less nutrients are left for the bacteria in the center to express any of the luxCDABE genes (either luciferase or luciferin substrates), which are the main contributors to the IVIS signal. This results in colony counts reaching a nearly steady-state as a function of time but expression level plateauing, causing an decay in IVIS signal due luciferase instability. We have previously modeled this scenario with a spatial model and a density dependent protein production term [1].

The rate of change of the luciferase enzymes is given by:

$$\frac{dL}{dt} = Bn_+\mu_+(1-\tau-\gamma_+/\mu_+) - \gamma_L L$$

where B represents the number of rate of expression of luciferase per cell and γ_L represents the luciferase decay. The IVIS signal (I) is proportional to the luciferase signal, i.e., I=κL, which scales parameters B and γ_L accordingly. The value of κ contains physical properties

such as the permitivity of skin to luciferase enzymes and number of photons emitted per enzyme. The lumped parameters chosen for the data presented in Figure 4 are: $\tau = 0.2, \kappa B = 10, A^+ = A^- = 0.01, K = 1000, \kappa\gamma_L = 0.3, \gamma_- = 0.001, \gamma_+ = 0.075, q = 1.6$ with initial conditions $n_+ = 3365, n_- = 0, I = 0, S = 1000$. Supplementary Figure 2 shows the substrate (all of Eq 3), growth rate for plasmid containing cells (Eq 4, teal), and substrate limitation function (right bracket Eq 3, green) as a function of time.

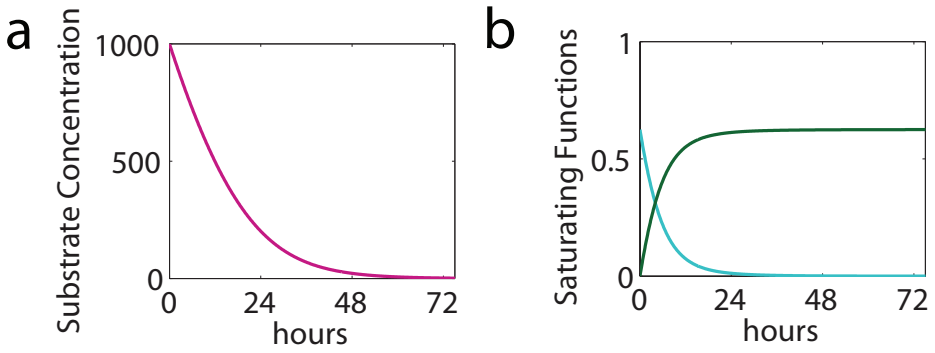

Figure 1: **a** Substrate concentration as a function of time for Figure4. **b** Saturating functions for the model. Green is the consumption of tumor substrate as a function of time. Teal is the growth rate of plasmid-containing cells as a function of time.

Model equations and parameter sets. Initially, an ODE system for plasmid loss was used that is similar to previous models [2]. One difference that arises in the tumor environment are that nutrients are spatially limited, hence consumption of tumor substrate is restricted to a certain number of bacteria. We accounted for this by limiting the substrate decay by total number of bacteria present. Several of the parameters are unknown, thus parameters were chosen to fit the bacterial population curves (Fig 2B) with growth rates and a loss rate close to experimental values. Then IVIS trajectories were generated using these fits. Quantitatively similar fits can be obtained by setting the growth rates equal and modifying the plasmid loss rate. Plasmid loss rate and a growth rate advantage of non-plasmid containing cells can compensate for one another, though experimentally we observe that non-plasmid containing cells grow faster in the tumor. This difference in growth rate may arise from the fact that newly formed non plasmid containing bacteria will occupy a larger percentage of cells on the growing front, allowing them to be in a more nutrient-available environment and grow faster as a population. This is also why we made the choice for non-plasmid containing cells degrading at a lower rate than the plasmid-containing ones.

References

[1] Danino, T., Mondragón-Palomino, O., Tsimring, L. & Hasty, J. A synchronized quorum of genetic clocks. *Nature* **463**, 326–330 (2010, PMID: 20090747).

[2] Ganusov, V., Bril kov, A. & Pechurkin, N. Mathematical modeling of population dynamics of unstable plasmid-bearing bacterial strains under continuous cultivation in a chemostat. *BIOPHYSICS-PERGAMON THEN MAIK NAUKA-C/C OF BIOFIZIKA* **45**, 881–887 (2000).

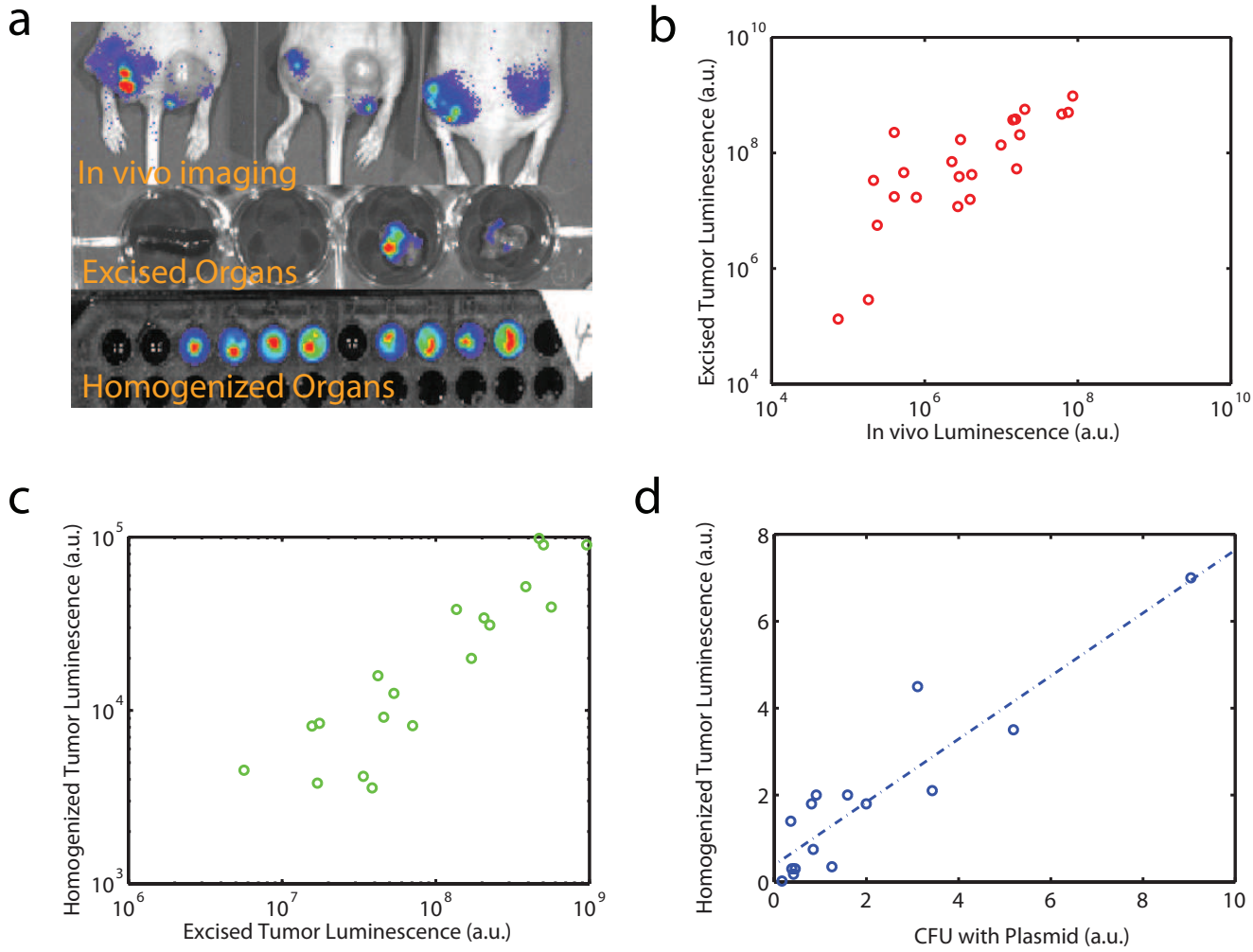

Figure 2: Correlations between in vivo and ex vivo imaging of tumors. High correlations are observed for each step of the process.

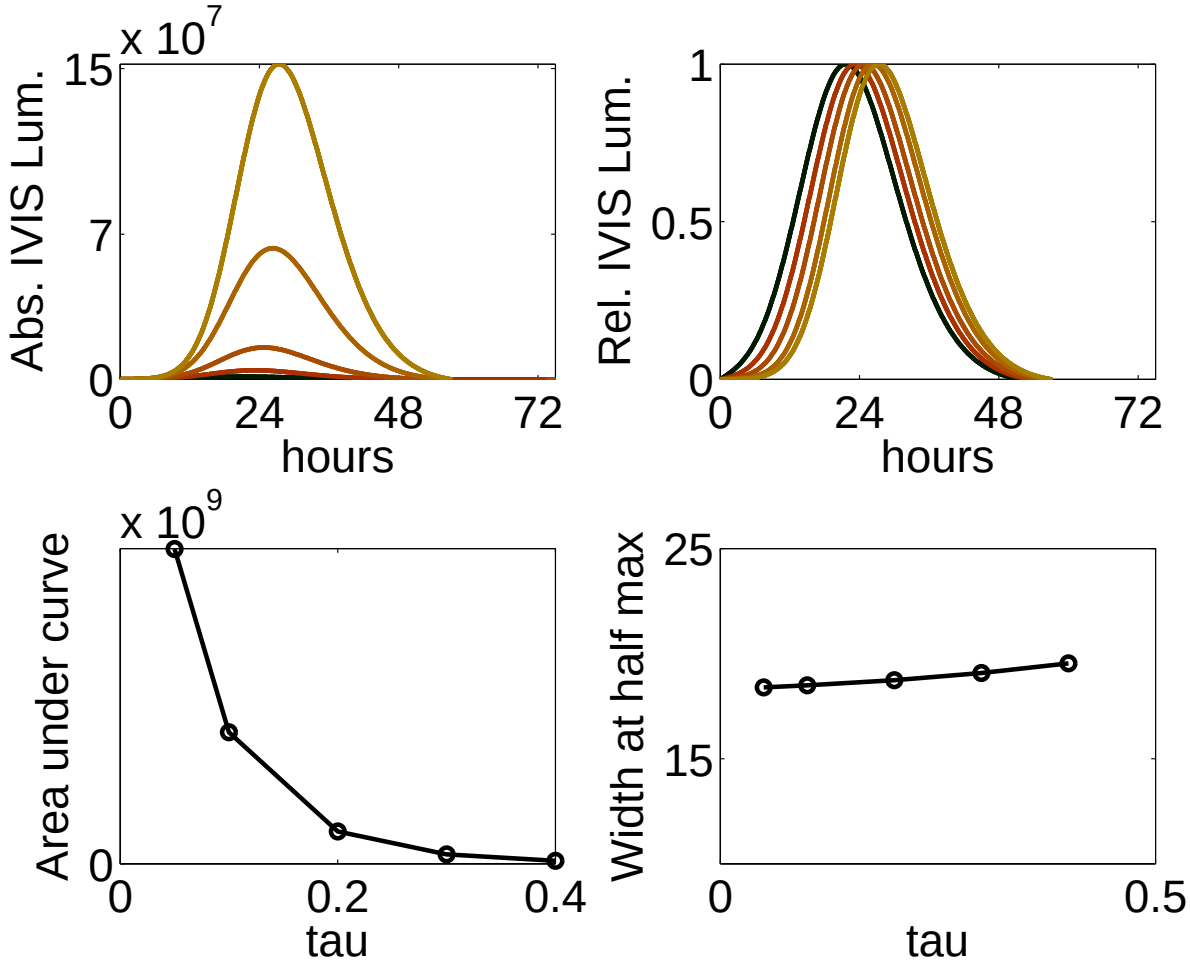

Figure 3: Effect of increasing τ on gene expression dynamics.